Advances in Science and Technology Research Journal

Advances in Science and Technology Research Journal 2024, 18(4), 23–32
https://doi.org/10.12913/22998624/188026
ISSN 2299-8624, License CC-BY 4.0

Received: 2024.04.24
Accepted: 2024.06.03
Published: 2024.06.20

Numerical Modelling of a Rotary Compression Test on a Cylindrical Specimen

Zbigniew Pater[1]

[1] Mechanical Faculty, Lublin University of Technology, ul. Nadbystrzycka 36, 20-618 Lublin, Poland
E-mail: z.pater@pollub.pl

ABSTRACT

This paper reviews studies on the modelling of the Mannesmann effect, which leads to the formation of an axial crack in parts formed by cross and skew rolling. This effect also occurs in the rotational compression (RC) test of a cylindrical specimen, which is used to determine the critical damage value. RC tests were carried out under laboratory conditions at the Lublin University of Technology on C45 steel specimens formed at 950 °C. Based on the tests, the crack propagation was presented as a function of the progress of rotational compression, measured by the length of the deformation path. The RC tests were numerically modelled in Forge® using four ductile fracture criteria. The effectiveness of the Mannesmann effect modelling was evaluated by comparing the numerically predicted cracks with the experimentally determined ones. In addition, the influence of an occurring axial crack on the stress state in the forming specimen was analysed.

Keywords: cracks, Mannesmann effect, FEM, experiment.

INTRODUCTION

Cross and skew rolling are among the metal forming techniques that have recently gained in popularity. These rolling methods have been used for many years in the production of preforms for drop forging [1–3] and stepped axles and shafts [4–6]. In addition, new manufacturing technologies are being developed on their basis [7–9], including the use of CNC rolling mills [10, 11].

The main problem with the widespread use of skew and cross rolling technology is the possibility of forming limitations such as necking (breakage), uncontrolled slippage and material cracking [12–14]. The most difficult problem is material cracking in the axial zone of the workpiece, commonly referred to as the Mannesmann effect. The essence of this effect is the creation of a stress state in the centre of the workpiece which, in combination with rotary motion, causes cyclic compressive and tensile stresses that lead to rapid crack nucleation due to separation of non-metallic inclusions from the metallic matrix. A further stage in the process is the growth of microcracks, which combine to form a macrocrack [15].

Previous numerical analyses to predict crack formation in a rolled part assumed material continuity, which significantly reduced the simulation time. The possibility of cracking was determined by analysing the distribution of the calculated damage function. If this function exceeded the critical damage value, the material was considered to be cracking. These analyses typically used universal fracture criteria for ductile materials implemented in the computer programs used [16–18]. In addition, several new damage criteria have been developed [19–22] which are specific to cross and skew rolling processes.

In several cases, modelling of crack initiation was also performed by deleting elements where the failure function exceeded a critical value. Such modelling was first carried out by Ceretti et al. [23] using the maximum principal stress criterion. More recently, Bulzak et al. [24] used this method to evaluate up to nine failure criteria for modelling cracking in the cross-rolling

process. However, the cited analyses were performed with a significant simplification, assuming a 2D plane strain state.

To summarise the analysis of the state of the art, no numerical simulation of Mannesmann effect cracking under 3D strain conditions has been performed to date. Therefore, a study in this area has been carried out. The results of this study are presented in this paper.

STUDY OBJECT – ROTARY COMPRESSION TEST OF A CYLINDRICAL SPECIMEN

The rotary compression (RC) process of a cylindrical specimen, which is used to calibrate the damage function [25], was chosen as the object of study. Figure 1 shows a schematic diagram of the RC process. It consists of deforming a cylindrical specimen of dimensions (Ø30 × 90 mm) with two flat tools, the lower of which is stationary and the upper of which moves linearly at a speed v. The distance between the tools is $2h$ and is less than the diameter of the specimen d_0. These parameters ensure that the upper tool grips the specimen and rolls it over the lower tool along a path of length s. As a result of the deformation, the cross-section of the specimen ovalises, leading to compressive and tensile stresses in the axial zone of the specimen which, for a suitable path length s, lead to the formation of a crack [26]. Determining the critical damage value in a rotary compression test involves experimentally determining the maximum path length s at which the material does not crack. The determined distance s is then used to model the numerically implemented RC case and to find the distribution of the damage function in the axial section of the rolled part. The maximum value of the determined function is considered to be the critical value of material damage.

EXPERIMENTAL TESTS

The rotational compression test was carried out under laboratory conditions at the Lublin University of Technology. A cross rolling mill was used in the tests, which allows rolling with tools of up to 1000 mm in length. Specimens of Ø30 × 90 mm, made of C45 grade steel, were formed. The distance between the tools was assumed to be $2h = 27.2$ mm.

The samples were heated in an electric furnace to $T_0 = 950$ °C. They were then placed on the lower stationary tool and formed with the upper tool moving at $v = 300$ mm/s (Fig. 2). In subsequent tests, the path s was successively increased (by 30 mm each time) until an axial crack appeared on the side surface of the workpiece, which occurred at $s = 250$ mm.

The specimens were then X-rayed to show the axial crack propagation due to the Mannesmann effect. The resulting radiographs, ordered by path s, are shown in Figure 3. This figure shows that crack propagation occurs rapidly over a path length s corresponding to a workpiece completing only one revolution. The crack appears in the centre of the specimen and propagates mainly in the axial direction to finally reach the entire length of the workpiece. At the same time, the crack increases in size transversely, resulting in a characteristic lenticular shape. The radiographs also show that the crack has a complex shape, consisting of a series of fractures that are also twisted.

NUMERICAL ANALYSIS

Numerical simulations of the RC test were carried out using the commercial software Forge®, which has been used repeatedly in the past to analyse cross and skew rolling processes [3, 9, 14, 27–31]. The results obtained from the

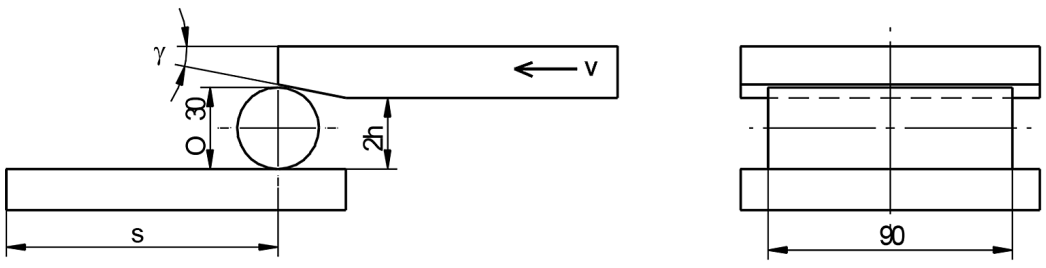

Figure 1. Diagram of the rotational compression (RC) test used to determine the critical value of material damage

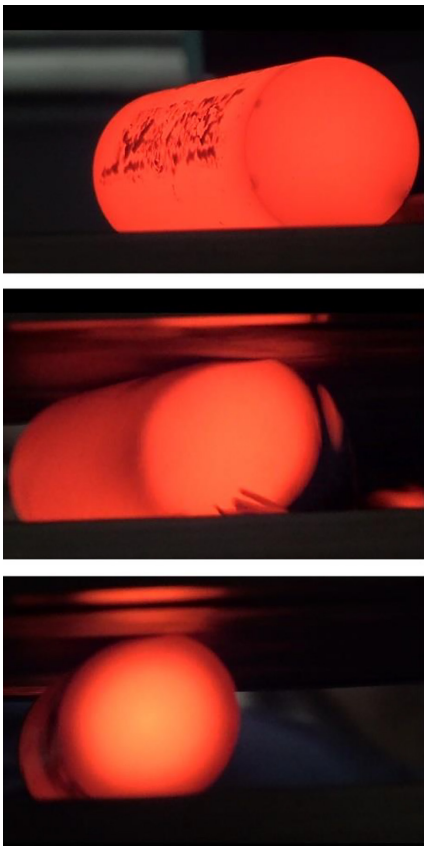

Figure 2. Rotational compression test of a cylindrical specimen at T = 950 °C and s = 250 mm.

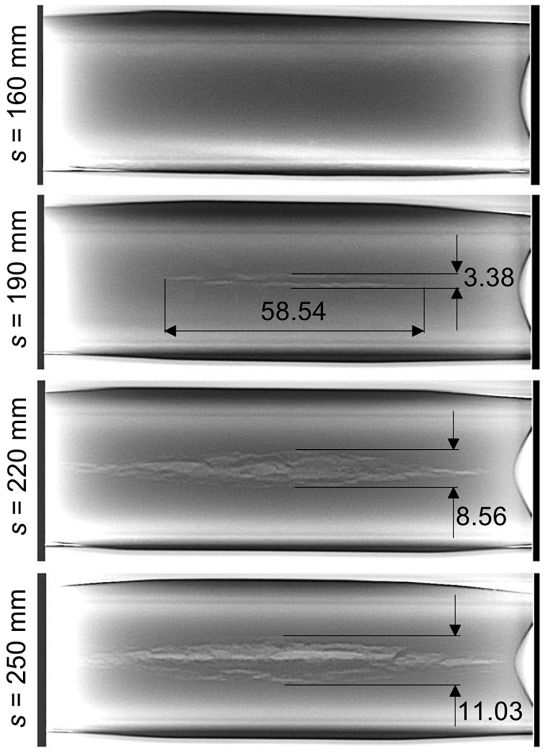

Figure 3. Radiograms of deformed specimens in a rotary compression test, realised with different forming path length s

simulations were in good agreement with the results of the experiments verifying them.

Figure 4 shows a geometric model of the analysed rotary compression case, taking into account the forming symmetries. The model consists of two perfectly rigid tools and a workpiece modelled as a plastic body. The lower tool is stationary, while the upper tool moves linearly at a speed of v = 300 mm/s. The workpiece is made of C45 steel, whose material model is described by the following Spittel Equation:

$$\sigma_f = 1521.31e^{-0.00269T}\varepsilon^{-0.12651}e^{\frac{-0.05957}{\varepsilon}}\dot{\varepsilon}^{0.14542} \quad (1)$$

where: σ_f – flow stress, ε – effective strain, $\dot{\varepsilon}$ – strain rate, T – temperature.

It has been assumed that the friction at the contact surface between the workpiece and the tools is described by the Tresca condition, according to which:

$$\tau = m\,k \quad (2)$$

where: τ – shear stress, k – shear yield strength ($k = \sigma_f/\sqrt{3}$), m – friction factor (assumed m = 0.8 [32]).

The calculations took into account the thermal phenomena occurring during forming, which were determined by the following parameters: billet and tool temperatures of 950 °C and 50 °C respectively, a heat transfer coefficient between the workpiece and tools of 10000 W/m^{2}K.

Four ductile fracture criteria were used to model the fracture of the material, from which the damage function f_i is calculated. These were:

- Oyane criterion

$$f_{OYAN} = \int_0^{\varepsilon_f} max\left(1 + 3\frac{\sigma_m}{\sigma_i}; 0\right)d\varepsilon \quad (3)$$

- Cockcroft and Latham criterion

$$\mathrm{f}_{CL} = \int_0^{\varepsilon_f} \sigma_1 d\varepsilon \quad (4)$$

- Normalised Cockcroft and Latham criterion

$$\mathrm{f}_{NCL} = \int_0^{\varepsilon_f} \frac{\sigma_1}{\sigma_i} d\varepsilon \quad (5)$$

- Rice and Tracey criterion

$$\mathrm{f}_{RT} = \int_0^{\varepsilon_f} C_1 e^{\left(C_2\frac{\sigma_m}{\sigma_i}\right)} d\varepsilon \quad (6)$$

In Equations 3–6 it is assumed that: ε_f – critical plastic strain at fracture, σ_i – equivalent stress, σ_m – hydrostatic stress, σ_1 – first principal stress, C_1 and C_2 – material constants, which are assumed

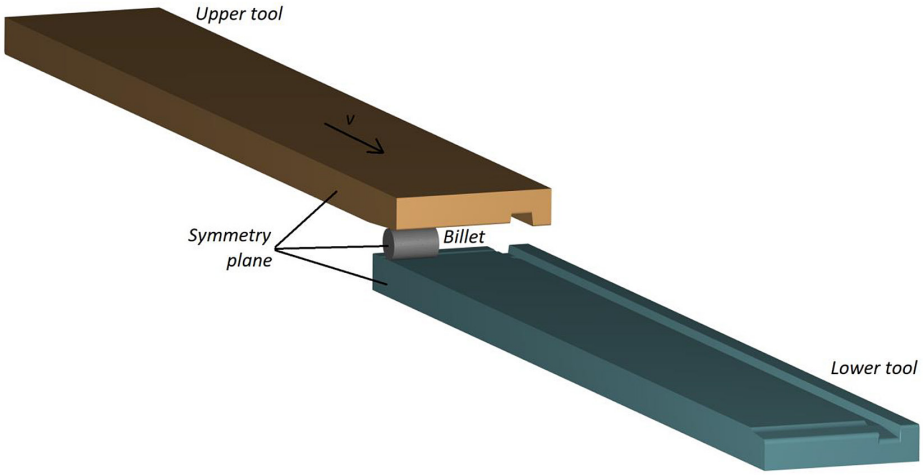

Figure 4. Geometrical model of the realised rotational compression test built in Forge® and taking into account the symmetry of forming

to be 0.283 and 1.5 respectively, according to the Forge® user manual.

The condition for fracture to occur is that the damage function f_i reaches the critical material damage value C_i, which can be expressed as follows:

$$f_i \geq C_i \tag{7}$$

In order to model material fracture in the RC test, it is necessary to have knowledge of the critical damage value, C_i. In order to determine this, the following methodology was adopted. First, the RC test was simulated without consideration of material fracture for a forming path of s = 160 mm, for which, according to Figure 3, no cracks were observed in the axial zone of the specimens. The maximum values of the damage function determined in this simulation were taken to be equal to the critical damage values, which for the adopted criteria were: C_{OYAN} = 3.052, C_{CL} = 161.4 MPa, C_{NCL} = 1.410, C_{RT} = 0.719. The RC test was then simulated again, this time taking into account the fracture of the material conditioned by the adopted damage criterion and the C_i value. The simulations were conducted with a forming path length of s = 250 mm, which corresponded to the maximum forming path length adopted in the experimental study.

Figures 5–7 show the cracks predicted numerically using the individual damage criteria, which are summarised for the different progression of the process conditioned by the length of the path s. Thus, Figure 3 shows the results obtained for a path s = 190 mm, at which a crack of 58.54 mm long and 3.38 mm wide was formed inside the specimen in the experimental tests. All of the criteria used predicted the occurrence of cracks that were, however, shorter and slightly wider than the crack determined experimentally. The best result was obtained using the Oyane criterion, for which the predicted crack length was 87.5% of the experimentally determined length. Slightly worse results were obtained using the Rice and Tracy criterion. It is noteworthy that in each case analysed, the crack had an identical shape, resembling an inverted letter S in cross section. This shape is undoubtedly a consequence of the circumferential flow of the material caused by the shear stresses. Figure 6 illustrates the predicted cracks for a forming path of s = 220 mm. These cracks are significantly shorter than the crack revealed in the experiment, which exhibited a characteristic lenticular shape and was propagated almost the entire length of the specimen (see Figure 3). With regard to the length of the predicted crack, it was the longest in the case where the Rice and Tracey criterion was applied. Additionally, the shape of the crack in cross-section underwent a transformation, taking on a cross-like configuration with curved arms. The predicted cracks along the maximum forming path of s = 250 mm are shown in Figure 7. In contrast to the experimental studies (Figure 3), no crack was formed along the entire length of the specimen in any of the cases analysed. It should be noted that the longest crack was predicted using the Rice and Tracey criterion, and that in all cases a crack width comparable to that observed in the experimental studies was obtained. The shape of the fracture in the cross-section became more complicated, as more spurs were added in

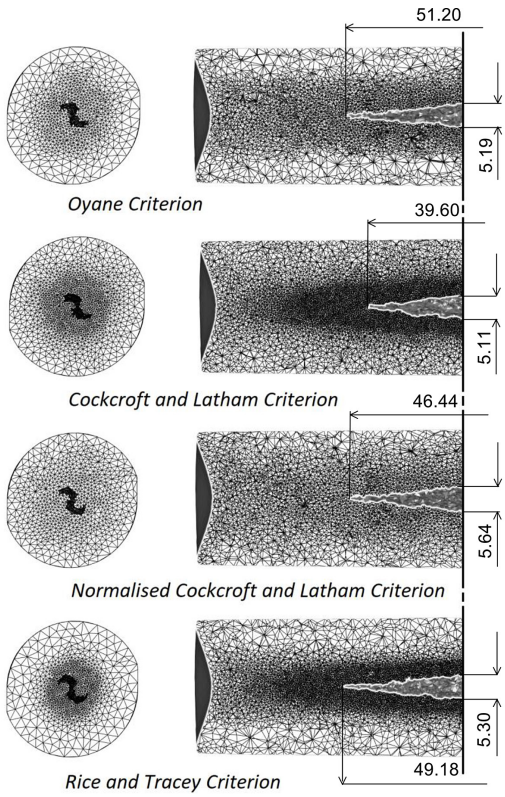

Figure 5. Numerically predicted cracks in a specimen deformed in the RC test over a path length of s=190 mm depending on the damage criterion used

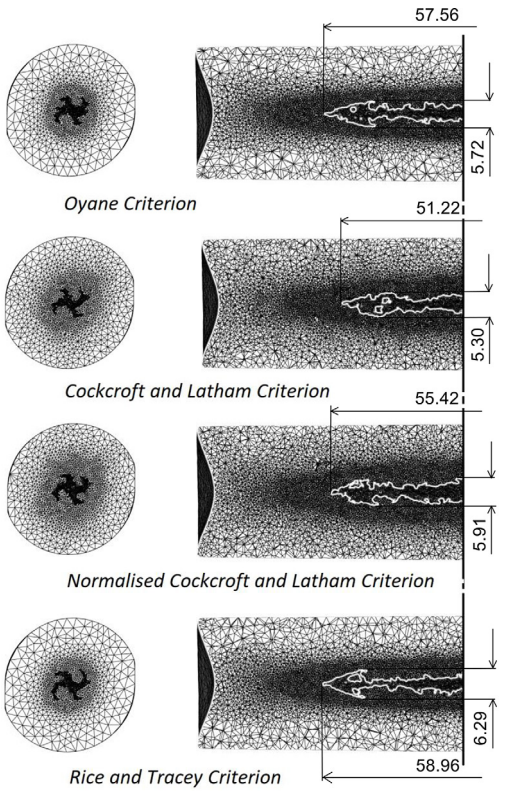

Figure 6. Numerically predicted cracks in a specimen deformed in the RC test over a path length of s=220 mm depending on the damage criterion used

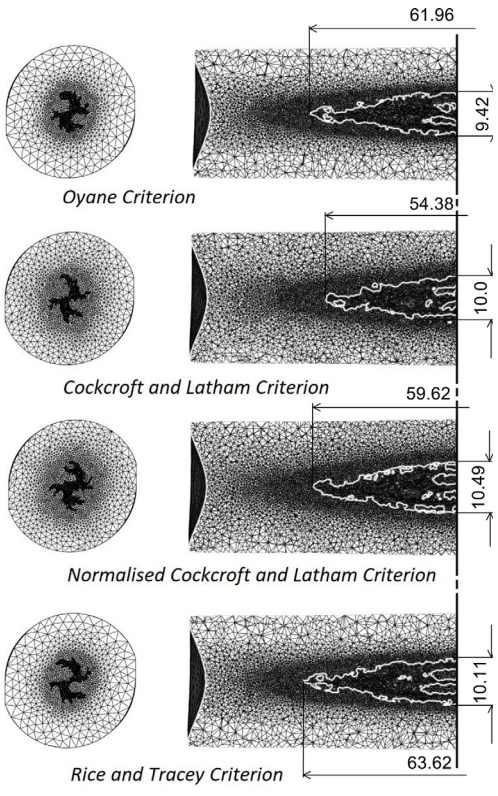

Figure 7. Numerically predicted cracks in a specimen deformed in the RC test over a path length of s=250 mm depending on the damage criterion used

the radial direction. Summarising the results of the numerical analysis of the Mannesmann effect, it can be concluded that the simulation of material fracture was consistent with the actual state only in the initial phase of fracture, when the crack occurred only in the centre of the specimen. The failure of the modelling of the crack propagation in the later crack phase, where it reached the entire length of the specimen, was probably due to the damage criteria adopted. As can be seen from Figure 8, the damage functions used took values close to 0 on the unloaded faces of the specimen, making it impossible to satisfy condition (7). In addition, crack propagation led to changes in the stress state (discussed below), which also led to a change in the critical failure value C_i.

A very important parameter used in fracture analysis is the stress triaxiality η defined as:

$$\eta \geq \frac{\sigma_m}{\sigma_i} \tag{8}$$

According to the study [33], when $\eta > 0.33$, fracture occurs by void nucleation, growth and coalescence. On the other hand, when $\eta < 0$, the loss of cohesion of the material occurs by shear, while in the case when $0 \leq \eta \leq 0.33$, both

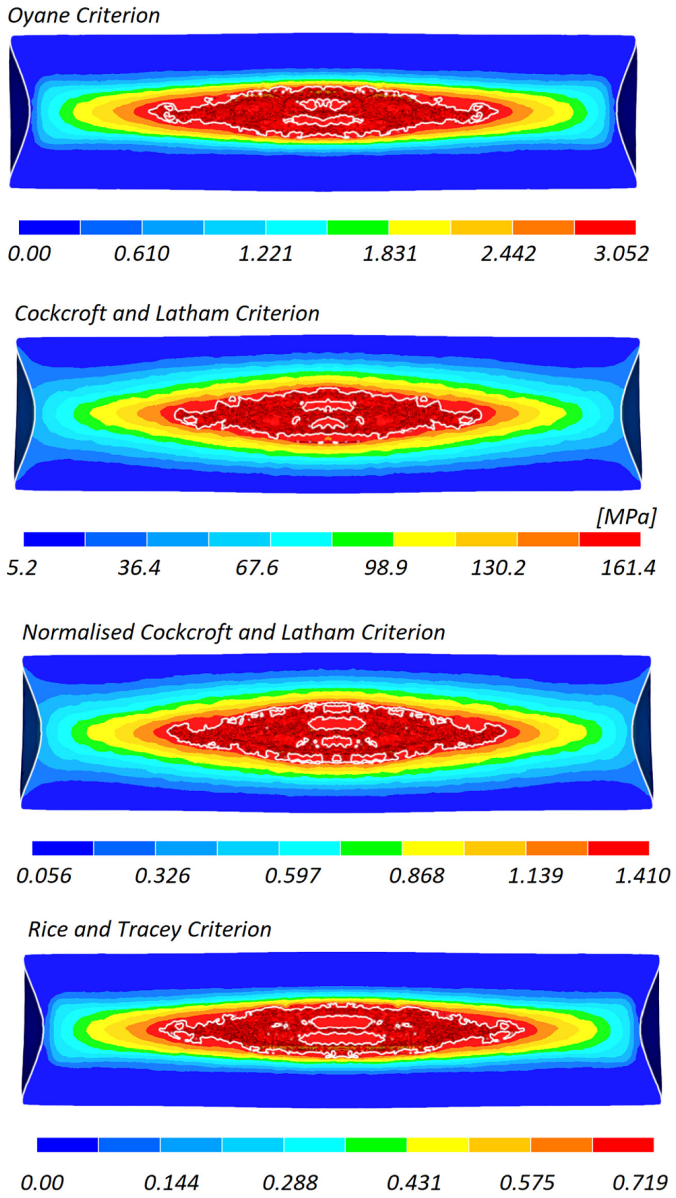

Figure 8. Numerically determined distribution of the damage function in the axial section of a specimen deformed in the RC test over a path length of s = 250 mm

mechanisms can take place. Furthermore, according to Bao and Wierzbicki [34], the material does not fracture at all when $\eta < -0.33$. In view of the above description, it is important to know how the parameter η is distributed in the axial section of a specimen subjected to rotational compression. According to Figure 9, until a crack appears, the stress state in the axis of the specimen is homogeneous and the values assumed by the parameter η indicate the possibility of crack formation due to both void nucleation and shear. A crack forming in the axial zone of the specimen radically changes the stress state, reducing the areas of high tensile stress to the corners of the crack where stress concentration takes place. The above observation is confirmed by the distribution of the first principal stress σ_1 shown in Figure 10. This stress is responsible for void nucleation and in the solid section reaches its highest values in the centre of the specimen where the crack initiates. In the subsequent fracture phase, stress σ_1 is responsible for crack propagation in the axial direction. The distribution of the maximum shear stress τ_{max} shown in Figure 11 is also interesting. This stress is responsible for the shear crack initiation and takes maximum values in the centre of the specimen where the crack initiates. After crack initiation, the distribution of τ_{max} changes significantly. The stress values decrease, probably due to the reduced stiffness of the specimen weakened by

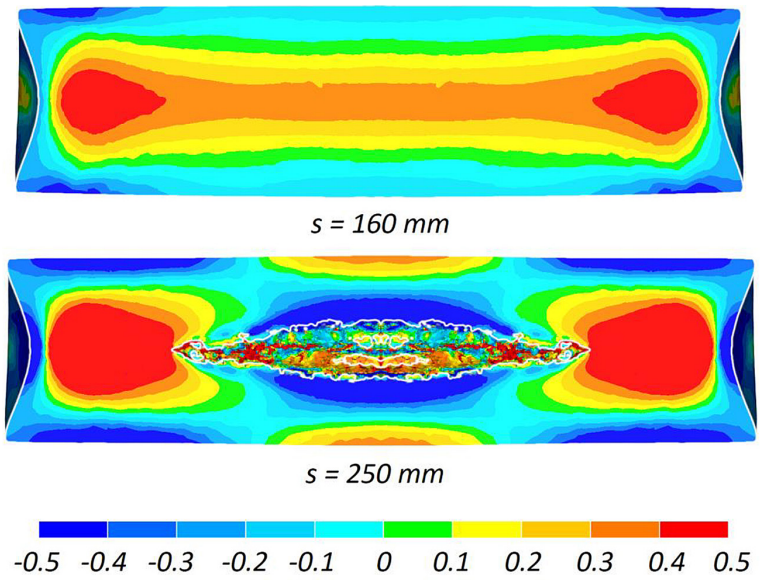

Figure 9. Numerically determined distribution of stress triaxiality η in the axial section of a specimen deformed in the RC test over a path length s (crack was determined using the Oyane criterion)

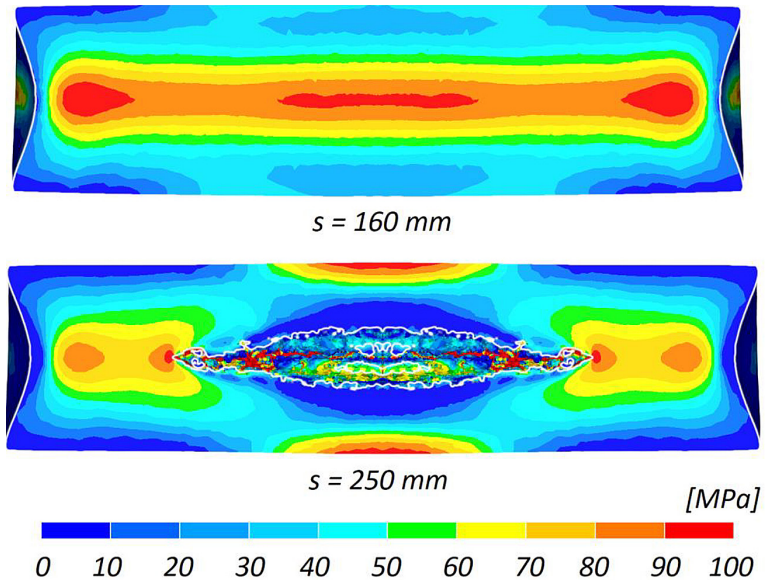

Figure 10. Numerically determined distribution of the first principal stress σ1 in the axial section of a specimen deformed in the RC test over a path length s (crack was determined using the Oyane criterion)

the resulting crack. The effect of τ_{max} in this phase of cracking is to curve the crack spurs, as can be seen in the cross sections of the specimens shown in Figures 5–7. The next Figure 12 shows the distribution of material temperature in the axial section of the specimen. This distribution shows that the material temperature increases in the centre of the specimen where the crack forms. This is due to the conversion of the work of plastic deformation into heat, which reaches its highest values in the axial zone of the specimen. On the other hand, there is a decrease in temperature in the layers close to the surface, from which heat is transferred to the much colder tools. An important parameter to consider in the numerical analysis is the computation time. Figure 13 shows diagrams illustrating the dependence of the CPU time on the damage criterion adopted and on the progress of the RC test, expressed by the displacement value *s*. All the compression cases analysed were carried out on the same computer and with the same element mesh parameters. The calculation

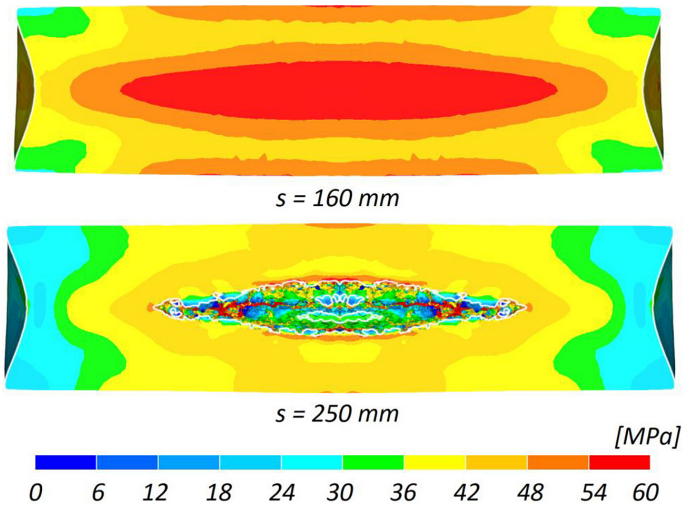

Figure 11. Numerically determined distribution of the maximum tangential stress τmax in the axial section of a specimen deformed in the RC test over a path length s (crack was determined using the Oyane criterion)

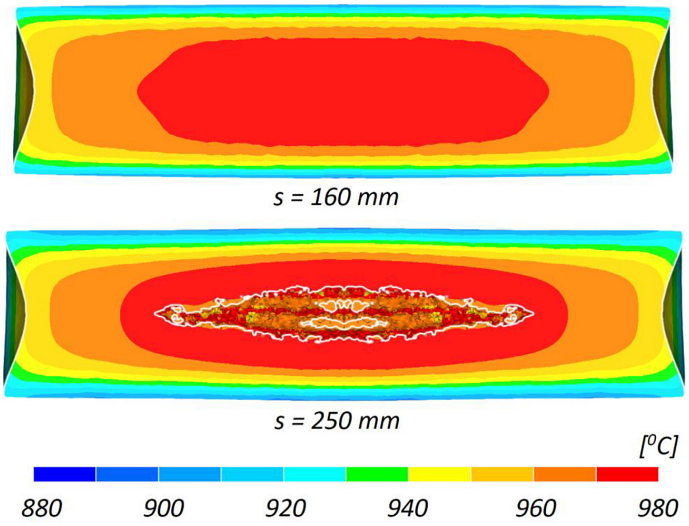

Figure 12. Numerically determined temperature distribution in the axial section of a specimen deformed in the RC test over a path length s (the crack was determined using the Oyane criterion)

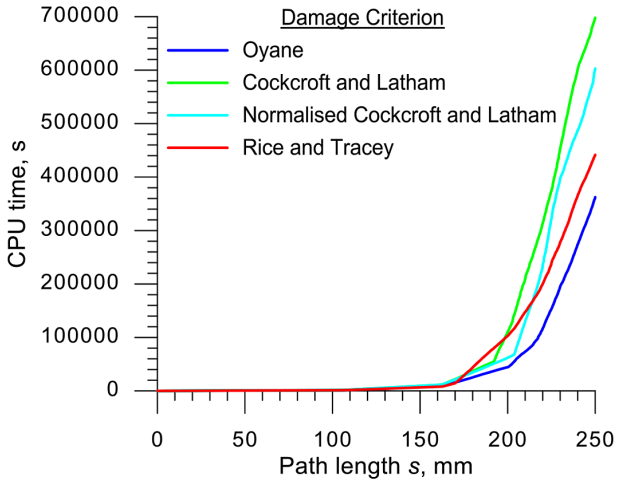

Figure 13. Effect of the damage criterion used on the simulation time of the RC test

time was the same in each case up to the point of cracking (s<160 mm). Significant time differences due to the damage criterion used were only recorded for the crack propagation simulation. The shortest CPU time was recorded when using the Oyane criterion and the longest when using the Cockcroft and Latham criterion ($t_{OYAN} = 0.52\ t_{CL}$).

CONCLUSIONS

On the basis of the experimental rotational compression tests performed on the cylindrical specimen and the numerical analysis carried out, the following conclusions were drawn:

- an axial crack is initiated at the centre of rotationally compressed cylindrical specimens;
- once initiated, the crack propagates axially until it reaches the full length of the specimen;
- Forge® software can be used to model axial crack initiation due to the Mannesmann effect;
- the accuracy of modelling the first crack phase (crack initiation) is assessed as good, but the accuracy of modelling the subsequent crack phase (crack propagation) is unsatisfactory;
- the emerging crack radically changes the stress state in the forming specimen, which consequently leads to a change in the critical damage value (keeping the critical damage value constant throughout the simulation is probably the reason for the unsatisfactory modelling results of the final crack phase);
- the best results for modelling the Mannesmann effect were obtained using the Oyane criterion.

REFERENCES

1. Meyer M., Stonis M., Behrens BA. Cross wedge rolling and bi-directional forging of preforms for crankshafts. Prod. Eng. Res. Devel. 2015, 9, 61–71. https://doi.org/10.1007/s11740-014-0581-8
2. Li P., Wang B., Feng P. et al. Numerical and experimental study on the hot cross wedge rolling of Ti-6Al-4V vehicle lower arm preform. Int. J. Adv. Manuf. Technol. 2022, 118, 3283–3301. https://doi.org/10.1007/s00170-021-07979-3
3. Pater Z., Tomczak J., Bulzak T., Walczuk-Gągała P. Numerical and experimental study on forming preforms in a CNC skew rolling mill. Archiv. Civ. Mech. Eng 2022, 22, e54. https://doi.org/10.1007/s43452-022-00373-0
4. Shen J., Wang B., Zhou J. et al. Numerical and experimental research on cross wedge rolling hollow shafts with a variable inner diameter. Archiv. Civ. Mech. Eng 2019, 19, 1497–1510. https://doi.org/10.1016/j.acme.2019.08.003
5. Pater Z., Tomczak J., Bulzak T. Numerical analysis of the skew rolling process for main shafts. Metalurgija 2015, 54(4), 627–630
6. Yang C., Ma J., Hu Z. Analysis and design of cross wedge rolling hollow axle sleeve with mandrel. J. Mater. Process. Tech. 2017, 239, 346–358. https://doi.org/10.1016/j.jmatprotec.2016.09.002
7. Huo Y., Bai Q., Wang B., Lin J., Zhou J. A new application of unified constitutive equations for cross wedge rolling of a high-speed railway axle steel. J. Mater. Process. Tech. 2015, 223, 274–283. https://doi.org/10.1016/j.jmatprotec.2015.04.011
8. Pater Z., Tomczak J., Bulzak T. New forming possibilities in cross wedge rolling processes. Archiv. Civ. Mech. Eng 2018, 18(1), 149–161. https://doi.org/10.1016/j.acme.2017.06.005
9. Pater Z., Tomczak J., Bulzak T., Cyganek Z., Andrietti S., Barbelet M. An innovative method for producing balls from scrap rail heads. Int. J. Adv. Manuf. Technol. 2018, 97, 893–901. https://doi.org/10.1007/s00170-018-2007-9
10. Tomczak J., Pater Z., Bulzak T., Lis K., Kusiak T., Sumorek A., Buczaj M. Design and technological capabilities of a CNC skew rolling mill. Archiv. Civ. Mech. Eng 2021, 21, 72. https://doi.org/10.1007/s43452-021-00205-7
11. Lin, L., Wang, B., Zhou, J. et al. Manufacturing large shafts by a novel flexible skew rolling process. Int. J. Adv. Manuf. Technol. 2022, 118, 2833–2851. https://doi.org/10.1007/s00170-021-08079-y
12. Pater Z., Weroński W., Kazanecki J., Gontarz A. Study of the process stability of cross wedge rolling. J. Mater. Process. Tech. 1999, 92–93, 458–462. https://doi.org/10.1016/S0924-0136(99)00229-0
13. Li Q., Lovell M. Cross wedge rolling failure mechanisms and industrial application. Int. J. Adv. Manuf. Technol. 2008, 37, 265–278. https://doi.org/10.1007/s00170-007-0979-y
14. Pater Z., Tomczak J., Bulzak T. Problems of forming stepped axles and shafts in a 3-roller skew rolling mill. J. Mater. Res. Technol. 2020, 9(5), 10434–10446. https://doi.org/10.1016/j.jmrt.2020.07.062
15. Yang C., Dong H., Hu Z. Micro-mechanism of central damage formation during cross wedge rolling. J. Mater. Process. Tech. 2028, 252, 322–332. https://doi.org/10.1016/j.jmatprotec.2017.09.041
16. Pater Z., Tomczak J., Bulzak T., Bartnicki J., Tofil A. Prediction of Crack Formation for Cross Wedge Rolling of Harrow Tooth Preform. Materials 2019, 12, 2287. https://doi.org/10.3390/ma12142287
17. Pater Z., Tomczak J., Bulzak T., Wójcik Ł., Walczuk P. Assessment of ductile fracture criteria with respect

to their application in the modeling of cross wedge rolling. J. Mater. Process. Tech. 2020, 278, 116501. https://doi.org/10.1016/j.jmatprotec.2019.116501

18. Bulzak T. Ductile fracture prediction in cross-wedge rolling of rail axles. Materials 2021, 14, 6638. https://doi.org/10.3390/ma14216638
19. Pater Z., Tomczak J., Bulzak T. Establishment of a new hybrid fracture criterion for cross wedge rolling. Int. J. Mech. Sci. 2020, 167, 105274. https://doi.org/10.1016/j.ijmecsci.2019.105274
20. Bulzak T., Pater Z., Tomczak J. Modified hybrid criterion for the cross wedge rolling process. J. Manuf. Process. 2023, 107, 496–505. https://doi.org/10.1016/j.jmapro.2023.10.075
21. Zhou X., Shao Z., Zhang C., Sun F., Zhou W., Hua L., Jiang J., Wang L. The study of central cracking mechanism and criterion in cross wedge rolling. Int. J. Mach. Tool. Manu. 2020, 159, 103647. https://doi.org/10.1016/j.ijmachtools.2020.103647
22. Yamane K., Shimoda K., Kuroda K., Kajikawa S., Kuboki T. A new ductile fracture criterion for skew rolling and its application to evaluate the effect of number of rolls. J. Mater. Process. Tech. 2021, 291, e116989. https://doi.org/10.1016/j.jmatprotec.2020.116989
23. Ceretti E., Giardini C., Attanasio A., Brisotto F., Capoferri G. Rotary Tube Piercing Study by FEM Analysis: 3D Simulation and Experimental Results. Tube and Pipe Technology, 2004, March/April, 155–159
24. Bulzak T., Wójcik Ł., Lis K., Kusiak T. Assessment of the possibility of quantitative identification of the Mannesmann effect using ductile fracture criteria. Int. J. Numer. Methods. Eng. 2024, e7430. https://doi.org/10.1002/nme.7430
25. Pater Z., Tomczak J., Bulzak T. Rotary compression as a new calibrating test for prediction of a critical damage value. J. Mater. Res. Technol. 2020, 9(3), 5487–5498. https://doi.org/10.1016/j.jmrt.2020.03.074
26. Pater Z., Walczuk P., Lis K., Wójcik Ł. Preliminary analysis of a rotary compression test. Adv. Sci. Technol. Res. J. 2018, 12(2), 77–82. https://doi.org/10.12913/22998624/86812
27. Bulzak T., Majerski K., Tomczak J., Pater Z., Wójcik Ł. Warm skew rolling of bearing steel balls using multiple impression tools. CIRP Journal of Manufacturing Science and Technology 2022, 38, 288–298. https://doi.org/10.1016/j.cirpj.2022.05.007
28. Tomczak J., Pater Z., Bulzak, T. A helical rolling process for producing ball studs. Archiv. Civ. Mech. Eng 2019, 19, 1316–1326. https://doi.org/10.1016/j.acme.2019.07.008
29. Derazkola H.A., Garcia E., Murillo-Marrodán A. Effects of skew rolling piercing process friction coefficient on tube twisting, strain rate and forming velocity. J. Mater. Res. Technol. 2023, 25, 7254–7272. https://doi.org/10.1016/j.jmrt.2023.07.167
30. Kruse J., Jagodzinski A., Langner J., Investigation of the joining zone displacement of cross-wedge rolled serially arranged hybrid parts. Int. J. Mater. Form. 2020, 13, 577–589. https://doi.org/10.1007/s12289-019-01494-3
31. Coors, T., Pape, F., Kruse, J., Stonis M., Behrens B.A. Simulation assisted process chain design for the manufacturing of bulk hybrid shafts with tailored properties. Int. J. Adv. Manuf. Technol. 2020, 108, 2409–2417. https://doi.org/10.1007/s00170-020-05532-2
32. Murillo-Marodan A., Garcia E., Cortes F. A study of friction model performance in a skew rolling process numerical simulation. Int. J. Simul. Model. 2018, 17(4), 569–582.
33. Li W., Liao F., Zhou T., Askes H. Ductile fracture of Q460 steel: Effects of stress triaxiality and Lode angle. J. Constr. Steel Res. 2016, 123, 1–17. https://doi.org/10.1016/j.jcsr.2016.04.018
34. Bao Y., Wierzbicki T. On the cut-off value of negative triaxiality for fracture. Eng. Fract. Mech. 2005, 72, 1049–1069. https://doi.org/10.1016/j.engfracmech.2004.07.011